Octadecanoids as emerging lipid mediators in cnidarian-dinoflagellate symbiosis

Marina T. Botana[1,2], Robert E. Lewis[1], Alessandro Quaranta[2], Olivier Salamin[2], Johanna Revol-Cavalier[2,3], Clint A. Oakley[1], Ivo Feussner[4], Mats Hamberg[2,3], Arthur R. Grossman[5], David J. Suggett[6], Virginia M. Weis[7], Craig E. Wheelock[2,8,*], Simon K. Davy[1,*]

[1]School of Biological Sciences, Victoria University of Wellington, Wellington 6012, New Zealand

[2]Unit of Integrative Metabolomics, Institute of Environmental Medicine, Karolinska Institutet, 171 77 Stockholm, Sweden.

[3]Larodan Research Laboratory, Karolinska Institutet, 171 65 Stockholm, Sweden.

[4]Department of Plant Biochemistry, Albrecht-von-Haller-Institute for Plant Sciences and Goettingen Center for Molecular Biosciences (GZMB), University of Goettingen, 37077 Goettingen, Germany

[5]Carnegie Institution for Science, Department of Plant Biology, Stanford, CA 94 305, USA

[6]KAUST Coral Restoration Initiative (KCRI) and Division of Biological and Environmental Science and Engineering (BESE), King Abdullah University of Science and Technology, Thuwal 23 955, Saudi Arabia

[7]Department of Integrative Biology, Oregon State University, Corvallis, OR 97331, USA

[8]Department of Respiratory Medicine and Allergy, Karolinska University Hospital, 171 76 Stockholm, Sweden.

*co-corresponding authors

Abstract

Oxylipin signaling has been suggested as a potential mechanism for the inter-partner recognition and homeostasis regulation of cnidarian-dinoflagellate symbiosis, which maintains the ecological viability of coral reefs. Here we assessed the effects of symbiosis and symbiont identity on a model cnidarian, the sea anemone *Exaiptasia diaphana*, using mass spectrometry to quantify octadecanoid oxylipins (*i.e.,* 18-carbon-derived oxygenated fatty acids). A total of 84 octadecanoids were reported, and distinct stereospecificity was observed for the synthesis of *R*- and *S*-enantiomers for symbiont-free anemones and free-living cultured dinoflagellate symbionts, respectively. Symbiont-derived 13(*S*)-hydroxy-octadecatetraenoic acid (13(*S*)-HOTE) linked to a 13*S*-lipoxygnase was translocated to the host anemone with a 32-fold increase, suggesting it as a biomarker of symbiosis and as a potential agonist of host receptors that regulate inflammatory transcription. Only symbiosis with the native symbiont *Breviolum minutum* decreased the abundance of pro-inflammatory 9(*R*)-hydroxy-octadecadienoic acid (9(*R*)-HODE) in the host. In contrast, symbiosis with the non-native symbiont *Durusdinium trenchii* was marked by higher abundance of autoxidation-derived octadecanoids, corroborating previous evidence for cellular stress in this association. The putative octadecanoid signaling pathways reported here suggest foundational knowledge gaps that can support the bioengineering and selective breeding of more optimal host-symbiont pairings to enhance resilience and survival of coral reefs.

Key words: Cell signaling, coral reef, Aiptasia, *Exaiptasia diaphana*, Symbiodiniaceae, zooxanthellae, lipoxygenase, octadecanoid, mass spectrometry, supercritical fluid chromatography

Introduction

Ecological success of coral reefs stems from the symbiotic relationship between the cnidarian host (*e.g.,* corals, sea anemones) and its dinoflagellate algal endosymbionts of the family Symbiodiniaceae. Evolution of this symbiosis over space and time has resulted in a high diversity of host and symbiont genotypes, as well as a high specificity of host-symbiont pairings and therefore, the occupation of distinct ecological niches by the holobiont (*i.e.,* the whole symbiosis)[1–3]. The symbiotic dinoflagellates supply their host with products from photosynthesis, including sugars, lipids and amino acids[4–6] and receive inorganic substrates and shelter from the host[7,8]. As in other symbiotic systems (*e.g.,* rhizobia-leguminous plants, human gut-microbiota), host-symbiont exchange not only involves nutritional compounds, but also cell signaling molecules that regulate inter-partner recognition and symbiosis function[9,10]. These signaling molecules might cross the symbiosome membrane, the host-derived vacuole membrane that encloses the dinoflagellate symbionts within the cnidarian host's gastrodermal cells, and which acts as the primary host-symbiont interface[11]. Glycans, small peptides, inositols, polar lipids, oxylipins and non-coding RNA have all been proposed as candidate signaling molecules that may interact with specific transmembrane transporters, enzyme-coupled receptors, and voltage-gated ion channels (*e.g.,* G-protein coupled receptors, lectins, peroxisome proliferator-activated receptors) for mediation of symbiosis establishment and cellular homeostasis; however, the underlying regulatory mechanisms involved in these processes remain poorly understood[12].

Oxylipins are a group of metabolites derived from oxygenated fatty acids that have gained recent attention in the cnidarian-dinoflagellate symbiosis[12,13], while also being reported as important bioactive mediators of cellular function and fate in many biological systems[14]. Oxylipins can be synthesized by the oxidation of mono- and polyunsaturated fatty acids (MUFA, PUFA) either following release from the cell membrane by lipase hydrolysis (*e.g.,* phospholipase A_2, PLA_2)[15] or by direct oxidation of the membrane lipids. They can also be formed by autoxidation processes (*e.g.*, *via* free radicals), which are not stereoselective[16] (**Fig. 1a**). Enzymatic formation of oxylipins is generally selective for carbon and double bond positions within the precursor fatty acid, so that only a specific regioisomer (*e.g.,* 9- or 13-hydroxy-octadecadienoic acid (HODE)) is synthesized by a given enzyme[17]. Biosynthesis of oxylipins is also often stereoselective[18], meaning that the geometrical configuration of the oxylipin product has a specific spatial 3D structure – for instance, either right-handed (the (*R*) enantiomer) or left-handed (the left (*S*) enantiomer) for molecules with only one chiral center[17] (**Fig.1b**). As such, determining the chirality of an oxylipin can indicate the synthetic source of the compound (*i.e.,* enzymatic or autoxidation). Determination of oxylipin biological function and regulation is aided by knowledge of the regio- and stereo-isomer configuration because the propagation of signaling cascades often relies on their interaction with stereoselective membrane receptors[19,20] (**Fig.1c**).

To date, only oxylipins derived from oxidation of 20-carbon fatty acids (*i.e.,* eicosanoids), particularly products of arachidonic acid (ARA, 20:4, n-6), have been suggested to exert key functions for host-symbiont communication in the cnidarian-dinoflagellate symbiosis[21–23]. Nevertheless, the high diversity of PUFA precursors, from both the host and symbiont, suggests that this symbiosis a promising model for exploration of novel oxylipins and the pathways responsible for their synthesis[13,24,25]. PUFA oxidation is mediated by the availability of both the substrate (*i.e.,* fatty acid) and initiator (*i.e.,* an oxygenating agent – enzymes, free radicals

or singlet oxygen), and by the scavenging capacity of the antioxidant machinery present in the biological system being studied. It is therefore necessary to explore the distribution of intact PUFAs and their modifying enzymes to better predict oxylipin profiles and their synthetic routes[26,27]. Stearidonic acid (SDA; 18:4, n-3) and octadecapentaenoic acid (ODPA; 18:5, n-3) are the most abundant PUFAs integral to the chloroplast membranes of the symbionts[13,28]. Oxylipins derived from 18-carbon fatty acids are termed octadecanoids[29] and have been primarily studied in plants, with the classical octadecanoid pathway critical for the formation of the phytohormone jasmonic acid (derived from α-linolenic acid, ALA 18:3, n-3)[30–32]. These ALA-derived metabolites are compounds of interest in the cnidarian-dinoflagellate symbiosis[33,34]. However, octadecanoids originating from SDA and ODPA are less studied and have only been reported to occur in cultures of Symbiodiniaceae[13]; their role in the cnidarian-dinoflagellate symbiosis remains unexplored.

Here we assessed the effects of symbiotic state and symbiont identity in the cnidarian-dinoflagellate symbiosis using a chiral supercritical fluid chromatography (SFC) coupled to tandem mass spectrometry (MS/MS) method to perform metabolic profiling of octadecanoids[35]. We used the sea anemone *Exaiptasia diaphana* (commonly called 'Aiptasia') as a host model, in symbiosis with either its native (homologous) symbiont *Breviolum minutum* or the non-native (heterologous) symbiont *Durusdinium trenchii*. This latter symbiont was chosen as it is a widely studied opportunist that provides less nutritional benefit to the host and induces cellular stress when it populates Aiptasia under experimental conditions[22,36]. Symbiont-free anemones (*i.e.,* aposymbiotic) and cultured symbionts were also analyzed to determine species specificity for the biosynthesis of specific oxylipin stereoisomers before addressing the impact of symbiotic state. Our comprehensive phenotypic analyses combined with top-down bioinformatics for determination of candidate biosynthetic enzymes of 18-carbon fatty acids enabled us to further describe the signaling cascades and pathways present in the cnidarian-dinoflagellate symbiosis and provide evidence for the inter-partner exchange of octadecanoids and their potential roles as lipid mediators.

Results

Distinct biosynthesis patterns in aposymbiotic anemones *vs.* cultured dinoflagellates

By chiral supercritical fluid chromatography (SFC) coupled to tandem mass spectrometry (MS/MS) (SFC-MS/MS), we were able to quantify 84 octadecanoids across all host and symbiont samples, including compounds derived from oleic acid (OA) (18:1, n-9), linoleic acid (LA) (18:2, n-6), alpha-linoleic acid (ALA) (18:3, n-3), gamma linoleic acid (GLA) (18:3, n-6) and stearidonic acid (SDA) (18:4, n-3). There was significant structural diversity in the detected octadecanoids; however, the overall concentrations of the different functional groups were in the order of mono-hydroxy>epoxy>oxo>trihydroxy>dihydroxy (**Fig. 3**; see **Fig. 2** for octadecanoid nomenclature). Diols derived from OA and ALA, as well as triols from ALA were absent from all sample groups (a detailed list of octadecanoids and their concentrations are provided in **Table S1**.

Aposymbiotic anemones and cultured dinoflagellates were first assessed for species-specificity with respect to the biosynthesis and potential origins of octadecanoids before evaluating the effects of symbiotic state. Differential stereochemistry specificity was observed (**Fig. 3a**), with

aposymbiotic anemones predominantly containing the (*R*) enantiomer of mono-hydroxy octadecanoids and cultured dinoflagellates the (*S*) enantiomer (**Fig. 3b and c**). Aposymbiotic anemones primarily produced (*R*) mono-hydroxylated forms of all regioisomers of SDA (*i.e.,* HOTEs), GLA (*i.e.,* HOTrEs-γ) and ALA (*i.e.,* HOTrEs). The observed stereoselectivity was determined using the % enantiomeric excess (ee), with values ranging from 64-100% (**Table S2**). Cultured *B. minutum* and *D. trenchii* exclusively contained the SDA-derived monohydroxy 13(*S*)-HOTE (**ee**=100%), consistent with enzymatic biosynthesis. In both dinoflagellate species, **ee** values also suggested the biosynthesis of the 13(*S*)-HOTrE enantiomer (**ee**=100% and 94% in *B. minutum* and *D. trenchii*, respectively) (**Table S2**). The only octadecanoid that exhibited the same stereospecificity for both aposymbiotic anemones and cultured dinoflagellates was 9(*R*),10(*S*),13(*R*)-TriHOME (**ee**=100% in all cases for position C-9) (**Table S2**).

Alterations in octadecanoid pathways in response to symbiotic state

Symbiont population densities in symbiotic anemones were not significantly different between the two dinoflagellate species (0.603±0.16 and 0.57±0.12 cells/ng host protein for *B. minutum* and *D. trenchii*, respectively). Any differences in the octadecanoid profile were therefore likely to be symbiont species-specific rather than a symbiont density effect. Profiling oxylipins with regio- and stereo-specificity enabled us to investigate alterations in distinct oxygenation pathways associated with symbiotic state and symbiont identity. There was a greater shift in the octadecanoid profile associated with symbiotic state (*i.e.*, symbiosis *vs*. aposymbiosis) than with symbiont identity (**Fig. 4**). Phenotypic remodeling was broadly manifested as upregulation of octadecanoids in both the host and symbiont when in symbiosis. Additionally, both partners showed lower ee values for multiple octadecanoid enantiomers when in symbiosis than in their isolated states (**Table S2**), with *S* enantiomers upregulated in the host and *R* enantiomers upregulated in the symbiont. Specifically, in symbiosis, the host exhibited an increased abundance of the 9(*R*),10(*S*),13(*R*)-TriHOME diastereoisomer and the (*S*) stereoisomers of HOTEs and HOTrEs-γ, with the biggest increases observed in *D. trenchii*-colonized anemones ($p<0.05$ with FDR) (**Fig. 5a**; **Table S3**). For EpODEs, EpOMEs and epoxy-HOMEs, an increase of up to 30-fold only occurred in anemones containing *D. trenchii* (**Tables S4**). In contrast, in *B. minutum*-colonized anemones, the level of 9(*R*)-HODE decreased 3-fold relative to aposymbiotic anemones **(Fig. 5a**). In the symbionts, the abundance of all octadecanoids except for 13(*S*)-HOTE was upregulated in symbiosis *vs.* culture, with most increases being more marked in *D. trenchii* than in *B. minutum* (**Fig. 5b**; **Table S5**). Increased enzymatic oxidation of ALA by 9-lipoxygenase (9-LOX) was evident for both dinoflagellate species. The abundance of HOTrEs from ALA was also elevated for both species. The abundance of Epoxy-HOMEs and EpODEs increased in both species, but in *D. trenchii* this increase was 3-fold greater than in *B. minutum* (**Fig. 5b** and **Table S5**).

Evidence for inter-partner exchange of octadecanoids

Aposymbiotic anemones did not contain 13(*S*)-HOTE, although this compound appeared in the host when colonized by either symbiont species, with the concentration 4-fold greater in anemones containing *D. trenchii* than those containing *B. minutum* (**Fig. 5a**; $p<0.05$, with

FDR). The (*S*) **ee** was 22% and 29% for anemones symbiotic with *B. minutum* and *D. trenchii*, respectively (**Fig. 5**). In comparison, the abundance of 13(*S*)-HOTE was significantly diminished in the symbiont when in symbiosis, in contrast to the pattern observed for all other octadecanoids (**Fig. 5b**; **Table S5**). The (*S*) **ee** values decreased from 100% to 10% in *B. minutum* and from 100% to 23% in *D. trenchii* in the symbiotic state (**Table S2**). These patterns suggest potential translocation from symbiont to host when in symbiosis.

Novel 9*S*- and 13*S*-lipoxygenases in Symbiodiniaceae

One *B. minutum* (MSTRG. 59407) and two *D. trenchii* (MSTRG.68745/7968) LOX-domain encoding mRNA sequences were proposed as novel LOX enzymes for Symbiodiniaceae (**Fig. 6**). The sequence for *B. minutum* was incomplete, but the alignment with AtLOX3 showed a combination of alanine and phenylalanine residues at the active site (**Fig. S2**), which revealed it as a 13*S*-LOX[41]. MSTRG.59407 had no blast hits with identity percentages above 79.9% in any of the searched public databases (*e.g.,* GeneBank, Reef Genomics and UNIPROT). The sequences for *D. trenchii* were 99.9% identical to two other sequences published in GenBank (CAK8999115.1 and CAK9070246.1), which have been described as "unnamed proteins". The alanine alignment and valine alignments with the active site residues of AtLOX 1 and 5 revealed that MSTRG.68745/7968 were 9*S*-LOXes (**Fig. S2**). All transcripts demonstrated active constitutive expression across both cultured and symbiotic Symbiodiniaceae RNA-seq datasets. Homology comparisons grouped the new Symbiodiniaceae LOXes within their own clade in the tree of life, being evolutionarily divergent from green algal (*i.e., Chlamydomonas reinhardtii* and *Lobosphera incisa*) and vascular plant LOXes, but rather closely related to a fungal Mn-LOX (**Fig. 6**).

Discussion

Interest in oxylipins as potential lipid mediators of inter-partner signaling in the cnidarian-dinoflagellate symbiosis has increased recently[12,13]. Here, octadecanoid biosynthesis by aposymbiotic anemones was found to be restricted to (*R)* enantiomers (as indicated by **ee** values of 100% for most HOTEs, HOTrEs and HOTrEs-γ). This trend was also reported for eicosanoid biosynthesis in various soft corals[37–40] and the stony corals *Acropora* sp. and *Galaxea fascicularis* [24]; however, the stereospecificity of octadecanoid formation in cnidarians was previously unknown. In contrast, octadecanoid biosynthesis in both the cultured homologous symbiont *Breviolum minutum* and the heterologous *Durusdinium trenchii* was restricted to (*S*) enantiomers, with 13(*S*)-HOTE and 13(*S*)-HOTrE especially prominent (**ee** values from 94-100%). Both compounds are likely formed *via* a 13(*S*)-lipoxygenase (LOX), which is enantioselective for the synthesis of (*S*) octadecanoids in the jasmonic acid pathway[41]. In microalgae, studies of the LOX pathways have primarily focused on the synthesis of eicosanoids and docosanoids (derived from 22-carbon fatty acids)[42–44], and there is a paucity of investigations of octadecanoid biosynthesis[45,46]. To our knowledge, this is the first study of LOX enzymes in Symbiodiniaceae and applied top-down bioinformatics to elucidate biosynthetic pathways in the cnidarian-dinoflagellate symbiosis.

Symbiosis resulted in increased levels of octadecanoids in both host and symbionts; however, there was a commensurate up to 3-fold decrease in their **ee** values. These findings suggest a

226 potential dynamic inter-partner exchange of compounds and/or alterations to symbiosis
227 homeostasis marked by a higher autoxidative state[47,48]. Specifically, *D. trenchii* promoted
228 greater abundance of octadecanoids in the host, consistent with a stress response, which was
229 further indicated by an up to 30-fold increase in epoxides (*i.e.,* EpODEs, EpOMEs and Epoxy-
230 HOMEs). In contrast, symbiosis with the homologous *B. minutum* resulted in only a slight
231 increase in octadecanoid abundance, which was more consistent with a homeostatic
232 adjustment. 9(*R*)-HODE has been linked to inflammation in mammals[49–51] and was exclusively
233 downregulated in *B. minutum*-colonized anemones, perhaps serving to dampen cellular stress
234 and so contribute to the persistence of this host-symbiont pairing[2,22]. A putative regulatory role
235 can be attributed to 9(*R*),10(*S*),13(*R*)-TriHOME (**ee**= 80% and 64% for position C-9, for
236 anemones with *B. minutum* and *D. trenchii*, respectively), for which the abundance increased
237 in symbiotic host tissues, although the associated pathway is unknown. In plants and humans,
238 TriHOMEs have been linked to lipoxygenases with species and tissue stereospecificity[52–55]. In
239 plants, TriHOMEs may also be linked to epoxyalcohol synthases (EAS), which together with
240 allene oxide synthase (AOS), are part of CYP74 in the cytochrome P450 family[41,56]. In
241 cnidarians, AOS and 8(*R*)-LOX genes have been linked to eicosanoid synthesis[39,57,58]; but
242 whether they are also involved in the synthesis of TriHOMEs and other octadecanoids remains
243 to be investigated, as does the potential synthesis role by EAS.

244 Symbiosis also led to a general increase in the abundance of octadecanoids in the symbiont,
245 with the greatest increase in *D. trenchii*. For both symbiont species, symbiosis caused changes
246 in the ALA oxidation pathway, possibly *via* one of the linoleate-LOXes described here. This
247 pathway occurs in plants[41], where synthesis of mono-hydroxy forms and a wide diversity of
248 ALA downstream products (*e.g.,* jasmonic acid and jasmonates) occurs in response to
249 wounding and necrotrophic fungal infection and recognition[59], as well as during network
250 communication in mycorrhiza[10,60]. The involvement of ALA oxidation products in host cell
251 invasion and/or host-symbiont communication in the cnidarian-dinoflagellate symbiosis is
252 therefore conceivable. However, the upregulation of LA and ALA oxidation pathways could
253 also be linked to oxidative stress, with the increased abundance of EpOMEs and EpODEs in
254 *D. trenchii* suggesting that this non-native symbiont species could be under greater cellular
255 stress than the native *B. minutum*. Such stress could have arisen due to the greater levels of
256 oxidative stress in the host's tissues discussed above, or perhaps other aspects of physiological
257 dysfunction associated with the poorer degree of host-symbiont integration that is typical of
258 this symbiotic pairing[2,22,61,62].

259

260 **Octadecanoids as putative mediators of lipid signaling**

261 Regulatory signaling involves both intracellular and intercellular cascades, and the
262 combination of both is crucial for endosymbioses[9,60,63,64]. In the cnidarian-dinoflagellate
263 symbiosis, intercellular signaling between the partners may occur *via* G-coupled receptors
264 associated with the symbiosome membrane[12,65], ultimately leading to alterations in host nuclear
265 transcription factors[66,67]; however, the molecular pathways involved are poorly understood[47,68].
266 In the case of intracellular signaling, a given molecule may bind to nuclear peroxisome
267 proliferator-activated receptors (PPAR) that also regulate transcriptional factors, such as
268 nuclear factor kappa-B (NF-kB) and tumor necrosis factors (TNF), mediators of inflammatory
269 and immune responses[64,69]. This latter mechanism has been widely studied in mammals but not

in the cnidarian-dinoflagellate symbiosis. Nevertheless, the expression of both NF-kB and TNF has been observed to change in the host in response to symbiosis, leading to the suggestion that they help regulate symbiosis stability[47,68].

The role of octadecanoids as PPAR ligands and controllers of transcriptional factors has received considerable attention in the biomedical field, and they have been extensively targeted for the development of metabolic regulatory drugs[70]. 13(*S*)-HODE and 9(*S*)-HODE are PPAR-γ ligands and controllers of the immune response in mammals, showing that different oxylipins can bind to the same receptor, although binding affinity is variable[70,71]. The SDA-derived octadecanoid 13(*S*)-HOTE, extracted from cultures of the green microalga *Chlamydomonas debaryana*, has also been shown to be a strong PPAR-γ ligand and to promote downregulation of NF-kB and other transcription factors in cell cultures and in a murine recurrent colitis model[72–74]. In our experimental system, the abundance of the symbiont-derived 13(*S*)-HOTE decreased in the symbiont fraction and increased in the host fraction while in symbiosis, supporting evidence for inter-partner communication *via* translocation of this compound. While confirmation is needed, our findings support this octadecanoid-receptor binding as a potential mechanism of host immune modulation. Transport of oxylipins through membranes often occurs through lipoproteins and we have previously reported these proteins to be 20-fold more abundant when Aiptasia is colonized with *B. minutum*[75]. Ultimately, oxylipin-receptor binding and translocation are promising themes for future research on the cnidarian-dinoflagellate symbiosis, with considerable potential to draw parallels with the biomedical field given that the cnidarian immune system is similar to that of higher organisms, including mammals[76].

Novel lipoxygenases in Symbiodiniaceae

We also studied the enzymatic candidates for the biosynthesis of 13(*S*) octadecanoids, which included a novel 13*S*-LOX for *B. minutum* and two 9*S*-LOXes for *D. trenchii*. In vascular plants, most 9-LOXes described to date are cytosolic and only free fatty acids serve as substrate, whereas 13-LOXes are either chloroplast-derived or cytosolic; and both esterified membranes or free fatty acids can serve as substrates[41]. 13-LOX activity forms the 13-positional mono-hydroperoxy fatty acids (*e.g.,* 13(*S*)-HpOTE and 13(*S*)-HpOTrE), whereas 9-LOXes synthesize the 9-positional forms (*e.g.,* 9(*S*)-HpOTE and 9(*S*)-HpOTrE)[77]. These fatty acid hydroperoxides can serve either as substrates for additional metabolic transformation (*e.g.,* AOS or EAS), or are reduced to form the corresponding mono-hydroxys (*e.g.,* HOTrEs or HOTEs). In cyanobacteria LOX, both positional mono-hydroxy forms can be synthesized by the same enzyme, because the insertion of molecular oxygen into the fatty acid chain is guided by steric shielding of the radical intermediate rather than by the positional orientation of the fatty acid when entering the enzyme active site[78]. We do not know which mechanism occurs in the Symbiodiniaceae, but the novel LOX identified in *B. minutum* is a candidate for the synthesis of symbiont-derived 13(*S*) octadecanoids. The active constitutive expression of both 13*S*- and 9*S*-LOX candidates across both cultured and symbiotic Symbiodiniaceae RNA-seq datasets also suggests that they might not only be real sequences, but also of paramount importance for symbiont metabolism.

In vascular plants, chloroplast-derived 13*S*-LOX has the highest substrate oxygenation kinetics with ALA[41,79], which is also true for LiLOX in the green alga *L. incisa*[80] and the

cyanobacterium *Cyanothece* sp.[78]. In plants, this initial oxygenation step is part of the jasmonic acid pathway, where jasmonic acid and other jasmonates help regulate the immune response, growth and development[31,81]. In Symbiodiniaceae, SDA and ODPA are more abundant than ALA[13,28], suggesting that their as yet unidentified downstream products might be key metabolic mediators and perhaps play a role in host-symbiont recognition. This hypothesis needs further investigation; however, it suggests that future studies should focus on ODPA-derived octadecanoids as well as oxylipins from 20-carbon and 22-carbon PUFAs to provide a broader understanding of the lipid signaling pathways present in the cnidarian-dinoflagellate symbiosis.

Conclusion

This work presents the first detailed quantification of octadecanoids in cnidarians and their associated symbionts. Determination of the octadecanoid stereochemistry provided insight into their biosynthetic route of formation. Our findings indicate a dynamic exchange of octadecanoids between symbiont and host and suggest that specific oxylipin stereoisomers act as putative lipid signaling mediators of this symbiosis. Understanding the molecular processes that underpin host-symbiont communication and symbiosis stability is of importance across symbiotic systems and is key in determining how to stabilize or strengthen host-symbiont interactions. For this purpose, the combination of lipidomics and reverse genetics is a powerful tool for further elucidation and discovery of new molecular pathways, which can contribute to our improved understanding of coral reef function. Accordingly, increased efforts should be made in understanding octadecanoid formation, endogenous levels, and signaling in relation to host-symbiont communication. This approach has the potential to improve the development of restoration and conservation tools involving bioengineering and selective breeding of more optimal host-symbiont pairings to enhance coral reef survival in the face of environmental stressors.

Material and methods

Maintenance of animal and algal cultures

Symbiodiniaceae cultures (*Breviolum minutum*, culture ID CCMP830; *Durusdinium trenchii*, culture ID D1A001 (see **Table S6** for species confirmation) were grown for eight years in f/2-enriched 0.22 µm filtered seawater (FSW)[82]. Culture flasks were maintained inside an incubator set to 25 °C (± 0.5 °C), under cool fluorescent lights (Osram Dulux 36/W890) at 90-110 µmol photons m^{-2} s^{-1} on a 12:12 h light/dark cycle.

Long-term clonal stocks of the sea anemone *Exaiptasia diaphana* (Aiptasia, culture ID: NZ1) were rendered aposymbiotic using a menthol protocol[83]. The anemones were confirmed to be aposymbiotic based on the absence of chlorophyll autofluorescence under confocal microscopy (Olympus Provis AX70; 100x magnification) and the absence of symbiont DNA amplification through polymerase chain reaction using ITS2_F and ITS_R primers[84]. Two thirds of the aposymbiotic stock (n = 150 anemones) were inoculated with either homologous *B. minutum* or heterologous *D. trenchii* and maintained in symbiosis for 15 months as described by Wuerz et al. (2023)[85]. All anemones were maintained in FSW and fed once a week with freshly hatched

355 *Artemia* sp. nauplii. Stocks were kept at 25 °C and 90-110 µmol photons m^{-2} s^{-1} on a 12:12 h
356 light/ dark cycle using Philips 6500K bulbs.

357

358 **Experimental setup**

359 Symbiodiniaceae cultures (n = 3 *per* species) were grown in 500 mL Erlenmeyer flasks under
360 the same conditions for long-term maintenance. Initial cell densities in flasks were
361 1000 cells per mL and culture growth was monitored using the confocal imaging system IN
362 Cell analyzer 6500 Hs, where cell density was quantified with Image J processing software (ten
363 counts *per* replicate). Cultures were monitored over time and sampling for octadecanoid
364 analysis occurred after 16 days, while the cultures were still in exponential growth (**Fig. S1**),
365 using sterile pipettes (150 mL *per* replicate). Samples were centrifuged at 4000 *g* for 5 min and
366 the resulting algal pellets flash-frozen and freeze-dried before storage at -80 °C in sterile 1.5
367 mL Eppendorf tubes. On the day of sampling, cultures were dark acclimated for 15 min within
368 4 h of initiating the light cycle, before measurements of 'photosynthetic health' (F_v/F_m) using
369 a Diving Pulse Amplitude Modulated Fluorometer (Diving-PAM, Walz, Effeltrich, Germany;
370 settings: measuring light = 4, saturation intensity = 8, saturation width = 0.8 s, gain = 3, and
371 damping = 3) (**Fig. S1**).

372 Anemones for each experimental treatment (*i.e.,* aposymbiotic; symbiotic with *B. minutum*;
373 and symbiotic with *D. trenchii*) were split across 3 x 400 mL jars *per* treatment (n = 15
374 anemones *per* jar) that contained FSW. These jars were then transferred to water baths set at
375 25 °C (± 0.5 °C) and under the same light conditions as described for the anemone stocks. All
376 anemones were fed with *Artemia* sp. nauplii at the same time of day and the old water was
377 changed with fresh FSW 8 h after feeding. Anemones were maintained under these conditions
378 for 16 days prior to sampling and analyses. On the sampling day, F_v/F_m of symbiotic anemones
379 was measured (**Fig. S1**) as described above for the Symbiodiniaceae cultures. Anemones (N =
380 10 *per* jar) were then pooled, washed, and homogenized with 1 mL of ice-cold 10 mM sodium
381 phosphate buffer (pH 7.4) containing 100 µM of the Fe chelator deferoxamine mesylate, using
382 a glass tissue grinder. Aposymbiotic anemone homogenates were flash-frozen, freeze-dried and
383 stored at -80 °C in 1.5 mL sterile Eppendorf tubes. Homogenates from pooled symbiotic
384 anemones were transferred to sterile Eppendorf tubes and centrifuged at 500 *g* for 5 min at 4
385 °C, to separate host and symbiont fractions. Host tissue supernatant was transferred to a
386 separate sterile tube and the pelleted symbiont dinoflagellate fraction was washed free of
387 residual host material by resuspension and centrifugation using the same buffer solution. A 20
388 µL aliquot of each host supernatant was analyzed for protein content using a fluorometric Qubit
389 Protein Assay Kit. After resuspension for a second time, the symbiont fraction was aliquoted
390 equally for cell counts, conducted using the confocal imaging system IN Cell analyzer 6500
391 Hs (as described above), and then normalized to host protein content (see Results). All steps
392 were performed on ice and final fractions were flash-frozen, freeze-dried and stored at -80 °C
393 until further analysis.

394

395 **Sample preparation and extraction**

396 Octadecanoids were extracted from freeze-dried biomass by adding 1.5 mL of methanol
397 (MeOH) and 10 µL of internal standard (IS) mix (**Table S7**). All samples were thoroughly

398 mixed by vortexing and subsequently sonicated in an ice bath for 30 min. Following
399 centrifugation for 10 min at 15,000 x *g* at 4 °C, the supernatant was transferred to a glass tube
400 and evaporated to dryness under nitrogen. To maximize compound recovery, this methanolic
401 extraction was repeated a second time and combined with the first extract. The dried extracts
402 were then reconstituted with 1 mL of a solution of 0.2 M Na_2HPO_4 and 0.1 M citric acid (pH
403 5.6). To concentrate the extract, solid phase extraction (SPE) was performed as described in
404 Quaranta et al. (2022), using an Extrahera automated sample preparation system (Biotage,
405 Uppsala, Sweden). Briefly, the 1 mL reconstituted extract was loaded onto a preconditioned 3
406 mL (3 cc/60 mg) Waters Oasis HLB cartridge (Milford, MA, USA). Samples were washed
407 three times with 3 mL of HPLC-grade water and a fourth time with 3 mL MeOH:H_2O (1:9).
408 Octadecanoids were eluted with 2.5 mL of MeOH and the extract was further evaporated to
409 dryness under a nitrogen stream. Reconstitution was performed with 80 µL MeOH, and the
410 samples were then filtered through a 0.1µm polyvinyldene fluoride membrane spin-filter
411 (Amicon, Merck Millipore Cooperation, Billerica, MA, USA) before being transferred to liquid
412 chromatography vials for analysis. Blanks comprised of FSW only, and culture medium was
413 added to ensure that oxylipin phenotypic profiles in samples were not related to possible
414 contamination from the experimental environment.

415

416 **Octadecanoid profiling and analysis**

417 A chiral supercritical fluid chromatography (SFC) coupled to tandem mass spectrometry
418 (MS/MS) platform was used to perform quantitative metabolic profiling of octadecanoids as
419 previously reported[35]. The published method was expanded by the addition of 27 novel custom
420 synthesized standards derived from oleic acid (OA), alpha-linolenic acid (ALA, n-3), gamma-
421 linolenic acid (GLA, n-6) and SDA (**Table S7**). The discrimination of *R* and *S* enantiomers for
422 the monohydroxy octadecanoids was based on the elution order in the chiral column following
423 the same patterns as observed for the 18 enantiopure standards detailed in Quaranta *et al.*
424 (2022)[35].

425 Extracts were first analyzed using the SFC method on a Waters UPC^2 system coupled to a
426 Waters Xevo TQ-XS mass spectrometer. Chiral separation was performed on a polysaccharide
427 Waters Trefoil AMY1 column (3.0x 150 mm, 2.5 µm) set at 35 °C and an injection volume of
428 2 µL. In addition to supercritical CO_2 as the main eluent (phase A), a co-modifier consisting of
429 MeOH:EtOH (8:2 by vol.) and CH_3COOH 0.1% v/v was used as phase B. The gradient started
430 with 5% B maintained until 1 min, before increasing it linearly to 25% B at 11 min and 30% B
431 at 12.3 min. The column was then washed with 50% B for 2-5 min and re-equilibrated under
432 the initial conditions for 2.2 min. Flow rate was 2.0 mL/min during separation and equilibration
433 but was decreased to 1.5 mL/min during washing. The active backpressure regulator (ABPR)
434 was set to 2000 psi and the make-up solvent consisting of MeOH and CH_3COONH_4 (5mM)
435 was flow rate-based on the co-modifier to avoid excess organic solvent at the source. It started
436 at a flow rate of 0.2 mL/min before linearly decreasing to 0 mL/min after 6 min.

437 The chromatographic system had an MS source operating in negative-ion ESI mode with a
438 capillary voltage of 1.9 kV, the source temperature at 150 °C, the desolvation temperature at
439 600 °C, the source offset at 30.0 V, the cone gas flow at 150 L h^{-1}, the desolvation gas flow at
440 1000 L h^{-1} and the nebulizer gas pressure at 7.0 bar. Negative multiple reaction monitoring
441 transitions along with the collision energy, cone voltage and dwell time were manually

442 optimized for each octadecanoid, and one transition *per* analyte was selected based upon
443 sensitivity and selectivity. Calibration was performed using an 11-point linear calibration
444 model, applying a 1/x weighted least-squared regression. Retrieved octadecanoid quantity was
445 normalized using the dry biomass, such that concentrations are reported in ng/g. MassLynx
446 software version 4.2 was used for data acquisition and TargetLynx for data processing.
447 Stereochemistry of the octadecanoids was evaluated using the enantiomeric excess (**ee**) (see
448 IUPAC compendium for chemical terminology). For each characterized regioisomer with
449 chiral configuration, the **ee** was calculated using the equation:

450 $$\% \text{ of } (R) \text{ or } (S) \text{ enantiomer} = 100 \times \text{total amounts of } (R) \text{ or } (S) / (R+S)$$

451

452 ***De novo* transcriptome assembly and mRNA expression quantification**

453 To describe the transcriptomic responses of both cultured and symbiotic *B. minutum* and *D.*
454 *trenchii*, a splice-aware transcriptome was assembled from previously sequenced RNA
455 libraries (Maor-Landaw *et al.,* 2019[86], BioProject: PRJNA544863 and Bellantuono *et al.,*
456 2019[87], BioProject PRJNA508937). Using Fastp[88], the raw paired-end RNA sequence files
457 were trimmed and filtered to remove sequencing adaptors and bases with Phred quality scores
458 below 30. Reads with more than 30% low-quality bases, containing more than 5 N bases, and
459 reads shorter than 50 bases after trimming were discarded.

460 Using the RNA-Seq aligner Spliced Transcripts Alignment to a Reference (STAR v2.7.10b[89]),
461 all filtered sample reads were first mapped without guidance to the Aiptasia genome (assembly
462 v1.1; GCF_001417965.1[90]) to filter anemone RNA reads and double mapping sequences for
463 downstream expression quantitation. Un-mapped RNA reads were collected and mapped
464 without guidance to the respective symbiont genomes of *B. minutum* (strain: Mf 1.05b.01;
465 GenBank assembly: GCA_000507305.1[91]) and *D. trenchii* (strain: CCMP2556;
466 GenBank assembly: GCA_963970005.1[92]). Splice-junction aware alignment outputs were
467 assembled into sample transcriptomes using StringTie2 v2.0.3[93]. Sample transcriptomes were
468 then merged into species RNA transcriptomes with a minimum transcript coverage of one
469 mapped read *per* base pair. All assembled RNA transcript open reading frames (ORFs) greater
470 than 100 amino acids were predicted using Transdecoder (TransDecoder.Predict v5.7, see
471 Github in references), to predict the most likely protein coding sequences (CDs regions) and
472 reduce the ORF false discovery rate. The ORFs were then filtered to retain only transcripts
473 with either Blastp protein sequence homology (e-value < $1e^{-5}$) to any described or hypothetical
474 protein in a collection of Stramenopile and Alveolate genomes (**Table S8**) and/or HMMER
475 (hmmscan v3.4) Pfam domain homology. Internal unique transcripts were used as training data
476 for the species-specific Markov Model-derived coding potential of the ORFs and to revise start
477 codon choice where statistically appropriate. After prediction, the best ORF candidates with
478 revised starts were propagated to each genome and written into new genomic protein-coding
479 transcript annotations.

480 To quantify transcript abundance and test for differential expression, un-normalized read
481 counts summarized at the gene (meta-feature) level for the homologous protein-coding
482 transcript annotations were performed on the RNA sequence STAR genomic alignments for
483 each sample, using FeatureCounts (Rsubread v2.16.1). All counted genes were tested for

484 differential expression among experimental conditions from the original raw datasets using
485 DeSeq2[94], with default internal gene-filtering procedures.

486

487 **Identification of Symbiodiniaceae LOX candidates and phylogeny**

488 To identify lipoxygenase (LOX) sequences in the protein-coding transcriptomes, a collection
489 of previously annotated LOX protein sequences, from both prokaryotic and eukaryotic species
490 was curated (**Table S9**). All hypothetical Symbiodiniaceae protein sequences were scanned for
491 sequence homology to the LOX references, using a Blastp cutoff of e-value = $1e^{-4}$. Presence of
492 Pfam LOX domains within the collection of Blastp candidates was confirmed with
493 InterProScan (interproscan.sh v5.68-101.0)[95]. Protein sequence phylogeny of the 13(*S*)-LOX
494 candidates was constructed from MUSCLE multiple sequence alignments, together with the
495 other LOX references[96]. The resulting distance matrix provided the information to generate a
496 phylogenetic tree using the neighbor-joining clustering method, with branch lengths optimized
497 *via* a phylogenetic maximum likelihood criterion[97], with Le and Gascuel model parameters[98].
498 The fitted tree was then bootstrapped 100 times.

499

500 **Statistical analysis**

501 Before evaluating the alterations caused by symbiotic state in both the host and symbiont,
502 oxylipin profiles of both aposymbiotic anemones and cultured dinoflagellates were
503 characterized, and symbiont species-specific compounds and the potential origins of
504 octadecanoid enantiomer biosynthesis patterns (*i.e., R* and/or *S*) were assessed by **ee** (**Table**
505 **S2**)**.** Principal component analysis (PCA) was used to identify the main differences in the
506 octadecanoid profiles associated with symbiotic state and symbiont identity, in the host and
507 symbiont separately. A two-way crossed ANOVA using symbiotic state (Symb; two levels in
508 the host: aposymbiotic and symbiotic; two levels in the symbiont: cultured and symbiotic)
509 orthogonal to the dinoflagellate species (Symb; two levels: *B. minutum* and *D. trenchii*) was
510 further applied for univariate validation of octadecanoids highlighted in the PCA. Additionally,
511 pairwise comparisons were analyzed with Tukey's HSD test, and the significance threshold set
512 at $p < 0.05$ with false discovery rate corrections. A volcano plot analysis that considered
513 pairwise fold-change differences of greater than two was also applied to the whole
514 octadecanoid matrix, to investigate whether oxidation pathways were altered due to the
515 symbiotic state in the host and symbiont. MetaboAnalyst version 6.0[99] was used for all
516 statistical analyses.

517

518

References

(1) Baker, A. C. Flexibility and Specificity in Coral-Algal Symbiosis: Diversity, Ecology, and Biogeography of *Symbiodinium*. *Annu. Rev. Ecol. Evol. Syst.* **2003**, *34* (1), 661–689. https://doi.org/10.1146/annurev.ecolsys.34.011802.132417.

(2) Gabay, Y.; Weis, V. M.; Davy, S. K. Symbiont Identity Influences Patterns of Symbiosis Establishment, Host Growth, and Asexual Reproduction in a Model Cnidarian-Dinoflagellate Symbiosis. *The Biological Bulletin* **2018**, *234* (1), 1–10. https://doi.org/10.1086/696365.

(3) Nitschke, M. R.; Rosset, S. L.; Oakley, C. A.; Gardner, S. G.; Camp, E. F.; Suggett, D. J.; Davy, S. K. The Diversity and Ecology of Symbiodiniaceae: A Traits-Based Review. In *Advances in Marine Biology*; Elsevier, 2022; Vol. 92, pp 55–127. https://doi.org/10.1016/bs.amb.2022.07.001.

(4) Muscatine, L. The Role of Symbiotic Algae in Carbon and Energy Flux in Reef Corals. *Coral reefs* **1990**.

(5) Papina, M.; Meziane, T.; van Woesik, R. Symbiotic Zooxanthellae Provide the Host-Coral Montipora Digitata with Polyunsaturated Fatty Acids. *Comparative Biochemistry and Physiology Part B: Biochemistry and Molecular Biology* **2003**, *135* (3), 533–537. https://doi.org/10.1016/S1096-4959(03)00118-0.

(6) Burriesci, M. S.; Raab, T. K.; Pringle, J. R. Evidence That Glucose Is the Major Transferred Metabolite in Dinoflagellate–Cnidarian Symbiosis. *Journal of Experimental Biology* **2012**, *215* (19), 3467–3477. https://doi.org/10.1242/jeb.070946.

(7) Weis, V. M. Cellular Mechanisms of Cnidarian Bleaching: Stress Causes the Collapse of Symbiosis. *Journal of Experimental Biology* **2008**, *211* (19), 3059–3066. https://doi.org/10.1242/jeb.009597.

(8) Davy, S. K.; Allemand, D.; Weis, V. M. Cell Biology of Cnidarian-Dinoflagellate Symbiosis. *Microbiol Mol Biol Rev* **2012**, *76* (2), 229–261. https://doi.org/10.1128/MMBR.05014-11.

(9) Beccaccioli, M.; Pucci, N.; Salustri, M.; Scortichini, M.; Zaccaria, M.; Momeni, B.; Loreti, S.; Reverberi, M.; Scala, V. Fungal and Bacterial Oxylipins Are Signals for Intra- and Inter-Cellular Communication within Plant Disease. *Front. Plant Sci.* **2022**, *13*, 823233. https://doi.org/10.3389/fpls.2022.823233.

(10) Liu, H.; Zhang, X.; Chen, W.; Wang, C. The Regulatory Functions of Oxylipins in Fungi: A Review. *J Basic Microbiol* **2023**, *63* (10), 1073–1084. https://doi.org/10.1002/jobm.202200721.

(11) Mashini, A. G.; Oakley, C. A.; Grossman, A. R.; Weis, V. M.; Davy, S. K. Immunolocalization of Metabolite Transporter Proteins in a Model Cnidarian-Dinoflagellate Symbiosis. *Appl Environ Microbiol* **2022**, *88* (12), e00412-22. https://doi.org/10.1128/aem.00412-22.

(12) Rosset, S. L.; Oakley, C. A.; Ferrier-Pagès, C.; Suggett, D. J.; Weis, V. M.; Davy, S. K. The Molecular Language of the Cnidarian–Dinoflagellate Symbiosis. *Trends in Microbiology* **2021**, *29* (4), 320–333. https://doi.org/10.1016/j.tim.2020.08.005.

(13) T. Botana, M.; Chaves-Filho, A. B.; Inague, A.; Z. Güth, A.; Saldanha-Corrêa, F.; Müller, M. N.; Sumida, P. Y. G.; Miyamoto, S.; Kellermann, M. Y.; Valentine, R. C.; Yoshinaga, M. Y. Thermal Plasticity of Coral Reef Symbionts Is Linked to Major Alterations in Their Lipidome Composition. *Limnology & Oceanography* **2022**, *67* (7), 1456–1469. https://doi.org/10.1002/lno.12094.

(14) Dyall, S. C.; Balas, L.; Bazan, N. G.; Brenna, J. T.; Chiang, N.; da Costa Souza, F.; Dalli, J.; Durand, T.; Galano, J.-M.; Lein, P. J.; Serhan, C. N.; Taha, A. Y. Polyunsaturated Fatty Acids and Fatty Acid-Derived Lipid Mediators: Recent Advances

in the Understanding of Their Biosynthesis, Structures, and Functions. *Progress in Lipid Research* **2022**, *86*, 101165. https://doi.org/10.1016/j.plipres.2022.101165.

(15) Dennis, E. A.; Deems, R. A.; Harkewicz, R.; Quehenberger, O.; Brown, H. A.; Milne, S. B.; Myers, D. S.; Glass, C. K.; Hardiman, G.; Reichart, D.; Merrill, A. H.; Sullards, M. C.; Wang, E.; Murphy, R. C.; Raetz, C. R. H.; Garrett, T. A.; Guan, Z.; Ryan, A. C.; Russell, D. W.; McDonald, J. G.; Thompson, B. M.; Shaw, W. A.; Sud, M.; Zhao, Y.; Gupta, S.; Maurya, M. R.; Fahy, E.; Subramaniam, S. A Mouse Macrophage Lipidome. *Journal of Biological Chemistry* **2010**, *285* (51), 39976–39985. https://doi.org/10.1074/jbc.M110.182915.

(16) Yin, H.; Xu, L.; Porter, N. A. Free Radical Lipid Peroxidation: Mechanisms and Analysis. *Chem. Rev.* **2011**, *111* (10), 5944–5972. https://doi.org/10.1021/cr200084z.

(17) Kuhn, H. Structural Basis for the Positional Specificity of Lipoxygenases. *Prostaglandins & Other Lipid Mediators* **2000**, *62* (3), 255–270. https://doi.org/10.1016/S0090-6980(00)00084-8.

(18) Stryer, L. Biochemistry. **1995**.

(19) Kolmert, J.; Fauland, A.; Fuchs, D.; Säfholm, J.; Gómez, C.; Adner, M.; Dahlén, S.-E.; Wheelock, C. E. Lipid Mediator Quantification in Isolated Human and Guinea Pig Airways: An Expanded Approach for Respiratory Research. *Anal. Chem.* **2018**, *90* (17), 10239–10248. https://doi.org/10.1021/acs.analchem.8b01651.

(20) Johnsson, A.-K.; Rönnberg, E.; Fuchs, D.; Kolmert, J.; Säfholm, J.; Claesson, H.-E.; Hamberg, M.; Wheelock, C. E.; Nilsson, G.; Dahlén, S.-E. COX-1 Dependent Biosynthesis of 15-Hydroxyeicosatetraenoic Acid in Human Mast Cells. *Biochimica et Biophysica Acta (BBA) - Molecular and Cell Biology of Lipids* **2021**, *1866* (5), 158886. https://doi.org/10.1016/j.bbalip.2021.158886.

(21) Hillyer, K. E.; Tumanov, S.; Villas-Bôas, S.; Davy, S. K. Metabolite Profiling of Symbiont and Host during Thermal Stress and Bleaching in a Model Cnidarian-Dinoflagellate Symbiosis. *Journal of Experimental Biology* **2015**, jeb.128660. https://doi.org/10.1242/jeb.128660.

(22) Matthews, J. L.; Crowder, C. M.; Oakley, C. A.; Lutz, A.; Roessner, U.; Meyer, E.; Grossman, A. R.; Weis, V. M.; Davy, S. K. Optimal Nutrient Exchange and Immune Responses Operate in Partner Specificity in the Cnidarian-Dinoflagellate Symbiosis. *PNAS* **2017**, *114* (50), 13194–13199. https://doi.org/10.1073/pnas.1710733114.

(23) Roach, T. N. F.; Dilworth, J.; H., C. M.; Jones, A. D.; Quinn, R. A.; Drury, C. Metabolomic Signatures of Coral Bleaching History. *Nat Ecol Evol* **2021**, *5* (4), 495–503. https://doi.org/10.1038/s41559-020-01388-7.

(24) Lõhelaid, H.; Samel, N. Eicosanoid Diversity of Stony Corals. *Marine Drugs* **2018**, *16* (1), 10. https://doi.org/10.3390/md16010010.

(25) Jónasdóttir, S. Fatty Acid Profiles and Production in Marine Phytoplankton. *Marine Drugs* **2019**, *17* (3), 151. https://doi.org/10.3390/md17030151.

(26) Coffa, G.; Brash, A. R. A Single Active Site Residue Directs Oxygenation Stereospecificity in Lipoxygenases: Stereocontrol Is Linked to the Position of Oxygenation. *Proc. Natl. Acad. Sci. U.S.A.* **2004**, *101* (44), 15579–15584. https://doi.org/10.1073/pnas.0406727101.

(27) Vecchio, A. J.; Simmons, D. M.; Malkowski, M. G. Structural Basis of Fatty Acid Substrate Binding to Cyclooxygenase-2. *Journal of Biological Chemistry* **2010**, *285* (29), 22152–22163. https://doi.org/10.1074/jbc.M110.119867.

(28) Sikorskaya, T. V.; Efimova, K. V.; Imbs, A. B. Lipidomes of Phylogenetically Different Symbiotic Dinoflagellates of Corals. *Phytochemistry* **2021**, *181*, 112579. https://doi.org/10.1016/j.phytochem.2020.112579.

(29) Quaranta, A.; Revol-Cavalier, J.; Wheelock, C. E. The Octadecanoids: An Emerging Class of Lipid Mediators. *Biochemical Society Transactions* **2022**, *50* (6), 1569–1582. https://doi.org/10.1042/BST20210644.

(30) Agrawal, G. K.; Tamogami, S.; Han, O.; Iwahashi, H.; Rakwal, R. Rice Octadecanoid Pathway. *Biochemical and Biophysical Research Communications* **2004**, *317* (1), 1–15. https://doi.org/10.1016/j.bbrc.2004.03.020.

(31) Wasternack, C. Jasmonates: An Update on Biosynthesis, Signal Transduction and Action in Plant Stress Response, Growth and Development. *Annals of Botany* **2007**, *100* (4), 681–697. https://doi.org/10.1093/aob/mcm079.

(32) Schaller, A.; Stintzi, A. Enzymes in Jasmonate Biosynthesis – Structure, Function, Regulation. *Phytochemistry* **2009**, *70* (13–14), 1532–1538. https://doi.org/10.1016/j.phytochem.2009.07.032.

(33) Lawson, C. A.; Possell, M.; Seymour, J. R.; Raina, J.-B.; Suggett, D. J. Coral Endosymbionts (Symbiodiniaceae) Emit Species-Specific Volatilomes That Shift When Exposed to Thermal Stress. *Sci Rep* **2019**, *9* (1), 17395. https://doi.org/10.1038/s41598-019-53552-0.

(34) Kim, T.; Baker, D. M.; Ju, S.-J.; Lee, J. C.-Y. Fatty Acid Profiles of Separated Host–Symbiont Fractions from Five Symbiotic Corals: Applications of Chemotaxonomic and Trophic Biomarkers. *Mar Biol* **2021**, *168* (11), 163. https://doi.org/10.1007/s00227-021-03979-9.

(35) Quaranta, A.; Zöhrer, B.; Revol-Cavalier, J.; Benkestock, K.; Balas, L.; Oger, C.; Keyes, G. S.; Wheelock, Å. M.; Durand, T.; Galano, J.-M.; Ramsden, C. E.; Hamberg, M.; Wheelock, C. E. Development of a Chiral Supercritical Fluid Chromatography–Tandem Mass Spectrometry and Reversed-Phase Liquid Chromatography–Tandem Mass Spectrometry Platform for the Quantitative Metabolic Profiling of Octadecanoid Oxylipins. *Anal. Chem.* **2022**, acs.analchem.2c02601. https://doi.org/10.1021/acs.analchem.2c02601.

(36) Starzak, D. E.; Quinnell, R. G.; Nitschke, M. R.; Davy, S. K. The Influence of Symbiont Type on Photosynthetic Carbon Flux in a Model Cnidarian–Dinoflagellate Symbiosis. *Mar Biol* **2014**, *161* (3), 711–724. https://doi.org/10.1007/s00227-013-2372-8.

(37) Brash, A. R.; Boeglin, W. E.; Chang, M. S.; Shieh, B.-H. Purification and Molecular Cloning of an 8R-Lipoxygenase from the Coral Plexaura Homomalla Reveal the Related Primary Structures of R- and S-Lipoxygenases. *Journal of Biological Chemistry* **1996**, *271* (34), 20949–20957. https://doi.org/10.1074/jbc.271.34.20949.

(38) Valmsen, K.; Järving, I.; Boeglin, W. E.; Varvas, K.; Koljak, R.; Pehk, T.; Brash, A. R.; Samel, N. The Origin of 15 *R* -Prostaglandins in the Caribbean Coral *Plexaura Homomalla* : Molecular Cloning and Expression of a Novel Cyclooxygenase. *Proc. Natl. Acad. Sci. U.S.A.* **2001**, *98* (14), 7700–7705. https://doi.org/10.1073/pnas.131022398.

(39) Lõhelaid, H.; Järving, R.; Valmsen, K.; Varvas, K.; Kreen, M.; Järving, I.; Samel, N. Identification of a Functional Allene Oxide Synthase-Lipoxygenase Fusion Protein in the Soft Coral Gersemia Fruticosa Suggests the Generality of This Pathway in Octocorals. *Biochimica et Biophysica Acta (BBA) - General Subjects* **2008**, *1780* (2), 315–321. https://doi.org/10.1016/j.bbagen.2007.10.010.

(40) Imbs, A. B.; Yakovleva, I. M.; Pham, L. Q. Distribution of Lipids and Fatty Acids in the Zooxanthellae and Host of the Soft Coral Sinularia Sp. *Fish Sci* **2010**, *76* (2), 375–380. https://doi.org/10.1007/s12562-009-0213-y.

(41) Wasternack, C.; Feussner, I. The Oxylipin Pathways: Biochemistry and Function. *Annu. Rev. Plant Biol.* **2018**, *69* (1), 363–386. https://doi.org/10.1146/annurev-arplant-042817-040440.

(42) Lamari, N.; Ruggiero, M. V.; d'Ippolito, G.; Kooistra, W. H. C. F.; Fontana, A.; Montresor, M. Specificity of Lipoxygenase Pathways Supports Species Delineation in the Marine Diatom Genus Pseudo-Nitzschia. *PLOS ONE* **2013**, *8* (8), e73281. https://doi.org/10.1371/journal.pone.0073281.
(43) d'Ippolito, G.; Nuzzo, G.; Sardo, A.; Manzo, E.; Gallo, C.; Fontana, A. Chapter Four - Lipoxygenases and Lipoxygenase Products in Marine Diatoms. In *Methods in Enzymology*; Moore, B. S., Ed.; Marine Enzymes and Specialized Metabolism - Part B; Academic Press, 2018; Vol. 605, pp 69–100. https://doi.org/10.1016/bs.mie.2018.02.021.
(44) Blasio, M.; Balzano, S. Fatty Acids Derivatives From Eukaryotic Microalgae, Pathways and Potential Applications. *Front. Microbiol.* **2021**, *12*. https://doi.org/10.3389/fmicb.2021.718933.
(45) Lang, I.; Feussner, I. Oxylipin Formation in Nostoc Punctiforme (PCC73102). *Phytochemistry* **2007**, *68* (8), 1120–1127. https://doi.org/10.1016/j.phytochem.2007.02.028.
(46) Lang, I.; Göbel, C.; Porzel, A.; Heilmann, I.; Feussner, I. A Lipoxygenase with Linoleate Diol Synthase Activity from *Nostoc* Sp. PCC 7120. *Biochemical Journal* **2008**, *410* (2), 347–357. https://doi.org/10.1042/BJ20071277.
(47) Lehnert, E. M.; Mouchka, M. E.; Burriesci, M. S.; Gallo, N. D.; Schwarz, J. A.; Pringle, J. R. Extensive Differences in Gene Expression Between Symbiotic and Aposymbiotic Cnidarians. *G3 Genes|Genomes|Genetics* **2014**, *4* (2), 277–295.
(48) Nielsen, D. A.; Petrou, K. Lipid Stores Reveal the State of the Coral-Algae Symbiosis at the Single-Cell Level. *ISME COMMUN.* **2023**, *3* (1), 29. https://doi.org/10.1038/s43705-023-00234-8.
(49) Bürger, F.; Krieg, P.; Kinzig, A.; Schurich, B.; Marks, F.; Fürstenberger, G. Constitutive Expression of 8-Lipoxygenase in Papillomas and Clastogenic Effects of Lipoxygenase-Derived Arachidonic Acid Metabolites in Keratinocytes. *Molecular Carcinogenesis* **1999**, *24* (2), 108–117. https://doi.org/10.1002/(SICI)1098-2744(199902)24:2<108::AID-MC5>3.0.CO;2-R.
(50) Cabral, M.; Martín-Venegas, R.; Moreno, J. J. Differential Cell Growth/Apoptosis Behavior of 13-Hydroxyoctadecadienoic Acid Enantiomers in a Colorectal Cancer Cell Line. *American Journal of Physiology-Gastrointestinal and Liver Physiology* **2014**, *307* (6), G664–G671. https://doi.org/10.1152/ajpgi.00064.2014.
(51) Vangaveti, V. N.; Jansen, H.; Kennedy, R. L.; Malabu, U. H. Hydroxyoctadecadienoic Acids: Oxidised Derivatives of Linoleic Acid and Their Role in Inflammation Associated with Metabolic Syndrome and Cancer. *European Journal of Pharmacology* **2016**, *785*, 70–76. https://doi.org/10.1016/j.ejphar.2015.03.096.
(52) Hamberg, M. An Epoxy Alcohol Synthase Pathway in Higher Plants: Biosynthesis of Antifungal Trihydroxy Oxylipins in Leaves of Potato. *Lipids* **1999**, *34* (11), 1131–1142. https://doi.org/10.1007/s11745-999-0464-7.
(53) Chiba, T.; Thomas, C. P.; Calcutt, M. W.; Boeglin, W. E.; O'Donnell, V. B.; Brash, A. R. The Precise Structures and Stereochemistry of Trihydroxy-Linoleates Esterified in Human and Porcine Epidermis and Their Significance in Skin Barrier Function. *Journal of Biological Chemistry* **2016**, *291* (28), 14540–14554. https://doi.org/10.1074/jbc.M115.711267.
(54) Fuchs, D.; Tang, X.; Johnsson, A.-K.; Dahlén, S.-E.; Hamberg, M.; Wheelock, C. E. Eosinophils Synthesize Trihydroxyoctadecenoic Acids (TriHOMEs) via a 15-Lipoxygenase Dependent Process. *Biochimica et Biophysica Acta (BBA) - Molecular and Cell Biology of Lipids* **2020**, *1865* (4), 158611. https://doi.org/10.1016/j.bbalip.2020.158611.

(55) Tyrrell, V. J.; Ali, F.; Boeglin, W. E.; Andrews, R.; Burston, J.; Birchall, J. C.; Ingram, J. R.; Murphy, R. C.; Piguet, V.; Brash, A. R.; O'Donnell, V. B.; Thomas, C. P. Lipidomic and Transcriptional Analysis of the Linoleoyl-Omega-Hydroxyceramide Biosynthetic Pathway in Human Psoriatic Lesions. *Journal of Lipid Research* **2021**, *62*, 100094. https://doi.org/10.1016/j.jlr.2021.100094.

(56) Brash, A. R. Mechanistic Aspects of CYP74 Allene Oxide Synthases and Related Cytochrome P450 Enzymes. *Phytochemistry* **2009**, *70* (13–14), 1522–1531. https://doi.org/10.1016/j.phytochem.2009.08.005.

(57) Koljak, R.; Boutaud, O.; Shieh, B.-H.; Samel, N.; Brash, A. R. Identification of a Naturally Occurring Peroxidase-Lipoxygenase Fusion Protein. *Science* **1997**, *277* (5334), 1994–1996. https://doi.org/10.1126/science.277.5334.1994.

(58) Lõhelaid, H.; Teder, T.; Tõldsepp, K.; Ekins, M.; Samel, N. Up-Regulated Expression of AOS-LOXa and Increased Eicosanoid Synthesis in Response to Coral Wounding. *PLoS ONE* **2014**, *9* (2), e89215. https://doi.org/10.1371/journal.pone.0089215.

(59) Battilani, P.; Lanubile, A.; Scala, V.; Reverberi, M.; Gregori, R.; Falavigna, C.; Dall'asta, C.; Park, Y.; Bennett, J.; Borrego, E. J.; Kolomiets, M. V. Oxylipins from Both Pathogen and Host Antagonize Jasmonic Acid-mediated Defence via the 9-lipoxygenase Pathway in *Fusarium Verticillioides* Infection of Maize. *Molecular Plant Pathology* **2018**, *19* (9), 2162–2176. https://doi.org/10.1111/mpp.12690.

(60) Niu, M.; Keller, N. P. Co-opting Oxylipin Signals in Microbial Disease. *Cellular Microbiology* **2019**, *21* (6), e13025. https://doi.org/10.1111/cmi.13025.

(61) Sproles, A. E.; Oakley, C. A.; Matthews, J. L.; Peng, L.; Owen, J. G.; Grossman, A. R.; Weis, V. M.; Davy, S. K. Proteomics Quantifies Protein Expression Changes in a Model Cnidarian Colonised by a Thermally Tolerant but Suboptimal Symbiont. *ISME J* **2019**, *13* (9), 2334–2345. https://doi.org/10.1038/s41396-019-0437-5.

(62) Medrano, E.; Merselis, D. G.; Bellantuono, A. J.; Rodriguez-Lanetty, M. Proteomic Basis of Symbiosis: A Heterologous Partner Fails to Duplicate Homologous Colonization in a Novel Cnidarian– Symbiodiniaceae Mutualism. *Front. Microbiol.* **2019**, *10*, 1153. https://doi.org/10.3389/fmicb.2019.01153.

(63) Bapaume, L.; Reinhardt, D. How Membranes Shape Plant Symbioses: Signaling and Transport in Nodulation and Arbuscular Mycorrhiza. *Front. Plant Sci.* **2012**, *3*. https://doi.org/10.3389/fpls.2012.00223.

(64) Wahli, W.; Michalik, L. PPARs at the Crossroads of Lipid Signaling and Inflammation. *Trends in Endocrinology & Metabolism* **2012**, *23* (7), 351–363. https://doi.org/10.1016/j.tem.2012.05.001.

(65) Peng, S.; Wang, Y.; Wang, L.; Chen, W. U.; Lu, C.; Fang, L.; Chen, C. Proteomic Analysis of Symbiosome Membranes in Cnidaria–Dinoflagellate Endosymbiosis. *Proteomics* **2010**, *10* (5), 1002–1016. https://doi.org/10.1002/pmic.200900595.

(66) Fraser, C. C. G Protein–Coupled Receptor Connectivity to NF-κB in Inflammation and Cancer. *International Reviews of Immunology* **2008**, *27* (5), 320–350. https://doi.org/10.1080/08830180802262765.

(67) Sun, L.; Ye, R. D. Role of G Protein-Coupled Receptors in Inflammation. *Acta Pharmacol Sin* **2012**, *33* (3), 342–350. https://doi.org/10.1038/aps.2011.200.

(68) Mansfield, K. M.; Carter, N. M.; Nguyen, L.; Cleves, P. A.; Alshanbayeva, A.; Williams, L. M.; Crowder, C.; Penvose, A. R.; Finnerty, J. R.; Weis, V. M.; Siggers, T. W.; Gilmore, T. D. Transcription Factor NF-κB Is Modulated by Symbiotic Status in a Sea Anemone Model of Cnidarian Bleaching. *Sci Rep* **2017**, *7* (1), 16025. https://doi.org/10.1038/s41598-017-16168-w.

(69) Liu, T.; Zhang, L.; Joo, D.; Sun, S.-C. NF-κB Signaling in Inflammation. *Sig Transduct Target Ther* **2017**, *2* (1), 17023. https://doi.org/10.1038/sigtrans.2017.23.

(70) Itoh, T.; Fairall, L.; Amin, K.; Inaba, Y.; Szanto, A.; Balint, B. L.; Nagy, L.; Yamamoto, K.; Schwabe, J. W. R. Structural Basis for the Activation of PPARγ by Oxidized Fatty Acids. *Nat Struct Mol Biol* **2008**, *15* (9), 924–931. https://doi.org/10.1038/nsmb.1474.

(71) Jagusch, H.; Werner, M.; Okuno, T.; Yokomizo, T.; Werz, O.; Pohnert, G. An Alternative Pathway to Leukotriene B_4 Enantiomers Involving a 1,8-Diol-Forming Reaction of an Algal Oxylipin. *Org. Lett.* **2019**, *21* (12), 4667–4670. https://doi.org/10.1021/acs.orglett.9b01554.

(72) Ávila-Román, J.; Talero, E.; Alcaide, A.; Reyes, C. D. L.; Zubía, E.; García-Mauriño, S.; Motilva, V. Preventive Effect of the Microalga *Chlamydomonas Debaryana* on the Acute Phase of Experimental Colitis in Rats. *Br J Nutr* **2014**, *112* (7), 1055–1064. https://doi.org/10.1017/S0007114514001895.

(73) Ávila-Román, J.; Talero, E.; de los Reyes, C.; García-Mauriño, S.; Motilva, V. Microalgae-Derived Oxylipins Decrease Inflammatory Mediators by Regulating the Subcellular Location of NFκB and PPAR-γ. *Pharmacological Research* **2018**, *128*, 220–230. https://doi.org/10.1016/j.phrs.2017.10.009.

(74) De Los Reyes, C.; Ávila-Román, J.; Ortega, M. J.; De La Jara, A.; García-Mauriño, S.; Motilva, V.; Zubía, E. Oxylipins from the Microalgae Chlamydomonas Debaryana and Nannochloropsis Gaditana and Their Activity as TNF-α Inhibitors. *Phytochemistry* **2014**, *102*, 152–161. https://doi.org/10.1016/j.phytochem.2014.03.011.

(75) Oakley, C. A.; Ameismeier, M. F.; Peng, L.; Weis, V. M.; Grossman, A. R.; Davy, S. K. Symbiosis Induces Widespread Changes in the Proteome of the Model Cnidarian *Aiptasia*: Symbiosis and the Aiptasia *Proteome*. *Cellular Microbiology* **2016**, *18* (7), 1009–1023. https://doi.org/10.1111/cmi.12564.

(76) Palmer, C. V.; Traylor-Knowles, N. Towards an Integrated Network of Coral Immune Mechanisms. *Proc. R. Soc. B.* **2012**, *279* (1745), 4106–4114. https://doi.org/10.1098/rspb.2012.1477.

(77) Newcomer, M. E.; Brash, A. R. The Structural Basis for Specificity in Lipoxygenase Catalysis: Specificity in Lipoxygenases. *Protein Science* **2015**, *24* (3), 298–309. https://doi.org/10.1002/pro.2626.

(78) Newie, J.; Andreou, A.; Neumann, P.; Einsle, O.; Feussner, I.; Ficner, R. Crystal Structure of a Lipoxygenase from Cyanothece Sp. May Reveal Novel Features for Substrate Acquisition [S]. *Journal of Lipid Research* **2016**, *57* (2), 276–287. https://doi.org/10.1194/jlr.M064980.

(79) Hofmann, E.; Zerbe, P.; Schaller, F. The Crystal Structure of *Arabidopsis Thaliana* Allene Oxide Cyclase: Insights into the Oxylipin Cyclization Reaction. *The Plant Cell* **2006**, *18* (11), 3201–3217. https://doi.org/10.1105/tpc.106.043984.

(80) Djian, B.; Hornung, E.; Ischebeck, T.; Feussner, I. The Green Microalga *Lobosphaera Incisa* Harbours an Arachidonate 15 *S* -lipoxygenase. *Plant Biol J* **2019**, *21* (S1), 131–142. https://doi.org/10.1111/plb.12920.

(81) Wasternack, C.; Hause, B. Jasmonates: Biosynthesis, Perception, Signal Transduction and Action in Plant Stress Response, Growth and Development. An Update to the 2007 Review in Annals of Botany. *Annals of Botany* **2013**, *111* (6), 1021–1058. https://doi.org/10.1093/aob/mct067.

(82) Guillard, R. R. L.; Ryther, J. H. STUDIES OF MARINE PLANKTONIC DIATOMS: I. CYCLOTELLA NANA HUSTEDT, AND DETONULA CONFERVACEA (CLEVE) GRAN. *Canadian Journal of Microbiology* **2011**. https://doi.org/10.1139/m62-029.

(83) Matthews, J. L.; Sproles, A. E.; Oakley, C. A.; Grossman, A. R.; Weis, V. M.; Davy, S. K. Menthol-Induced Bleaching Rapidly and Effectively Provides Experimental

Aposymbiotic Sea Anemones (*Aiptasia* Sp.) for Symbiosis Investigations. *Journal of Experimental Biology* **2015**, jeb.128934. https://doi.org/10.1242/jeb.128934.

(84) Goulet, T.; Coffroth, M. Genetic Composition of Zooxanthellae between and within Colonies of the Octocoral Plexaura Kuna, Based on Small Subunit rDNA and Multilocus DNA Fingerprinting. *Marine Biology* **2003**, *142* (2), 233–239. https://doi.org/10.1007/s00227-002-0936-0.

(85) Wuerz, M.; Lawson, C. A.; Oakley, C. A.; Possell, M.; Wilkinson, S. P.; Grossman, A. R.; Weis, V. M.; Suggett, D. J.; Davy, S. K. Symbiont Identity Impacts the Microbiome and Volatilome of a Model Cnidarian-Dinoflagellate Symbiosis. *Biology* **2023**, *12* (7), 1014. https://doi.org/10.3390/biology12071014.

(86) Maor-Landaw, K.; Oppen, M. J. H.; McFadden, G. I. Symbiotic Lifestyle Triggers Drastic Changes in the Gene Expression of the Algal Endosymbiont *Breviolum Minutum* (Symbiodiniaceae). *Ecol Evol* **2020**, *10* (1), 451–466. https://doi.org/10.1002/ece3.5910.

(87) Bellantuono, A. J.; Dougan, K. E.; Granados-Cifuentes, C.; Rodriguez-Lanetty, M. Free-living and Symbiotic Lifestyles of a Thermotolerant Coral Endosymbiont Display Profoundly Distinct Transcriptomes under Both Stable and Heat Stress Conditions. *Mol Ecol* **2019**, *28* (24), 5265–5281. https://doi.org/10.1111/mec.15300.

(88) Chen, S.; Zhou, Y.; Chen, Y.; Gu, J. Fastp: An Ultra-Fast All-in-One FASTQ Preprocessor. *Bioinformatics* **2018**, *34* (17), i884–i890. https://doi.org/10.1093/bioinformatics/bty560.

(89) Dobin, A.; Davis, C. A.; Schlesinger, F.; Drenkow, J.; Zaleski, C.; Jha, S.; Batut, P.; Chaisson, M.; Gingeras, T. R. STAR: Ultrafast Universal RNA-Seq Aligner. *Bioinformatics* **2013**, *29* (1), 15–21. https://doi.org/10.1093/bioinformatics/bts635.

(90) Baumgarten, S.; Bayer, T.; Aranda, M.; Liew, Y. J.; Carr, A.; Micklem, G.; Voolstra, C. R. Integrating microRNA and mRNA Expression Profiling in Symbiodinium Microadriaticum, a Dinoflagellate Symbiont of Reef-Building Corals. *BMC Genomics* **2013**, *14* (1), 704. https://doi.org/10.1186/1471-2164-14-704.

(91) Shoguchi, E.; Shinzato, C.; Kawashima, T.; Gyoja, F.; Mungpakdee, S.; Koyanagi, R.; Takeuchi, T.; Hisata, K.; Tanaka, M.; Fujiwara, M.; Hamada, M.; Seidi, A.; Fujie, M.; Usami, T.; Goto, H.; Yamasaki, S.; Arakaki, N.; Suzuki, Y.; Sugano, S.; Toyoda, A.; Kuroki, Y.; Fujiyama, A.; Medina, M.; Coffroth, M. A.; Bhattacharya, D.; Satoh, N. Draft Assembly of the Symbiodinium Minutum Nuclear Genome Reveals Dinoflagellate Gene Structure. *Current Biology* **2013**, *23* (15), 1399–1408. https://doi.org/10.1016/j.cub.2013.05.062.

(92) Dougan, K. E.; Bellantuono, A. J.; Kahlke, T.; Abbriano, R. M.; Chen, Y.; Shah, S.; Granados-Cifuentes, C.; Van Oppen, M. J. H.; Bhattacharya, D.; Suggett, D. J.; Rodriguez-Lanetty, M.; Chan, C. X. Whole-Genome Duplication in an Algal Symbiont Bolsters Coral Heat Tolerance. *Sci. Adv.* **2024**, *10* (29), eadn2218. https://doi.org/10.1126/sciadv.adn2218.

(93) Kovaka, S.; Zimin, A. V.; Pertea, G. M.; Razaghi, R.; Salzberg, S. L.; Pertea, M. Transcriptome Assembly from Long-Read RNA-Seq Alignments with StringTie2. *Genome Biol* **2019**, *20* (1), 278. https://doi.org/10.1186/s13059-019-1910-1.

(94) Love, M. I.; Huber, W.; Anders, S. Moderated Estimation of Fold Change and Dispersion for RNA-Seq Data with DESeq2. *Genome Biol* **2014**, *15* (12), 550. https://doi.org/10.1186/s13059-014-0550-8.

(95) Jones, P.; Binns, D.; Chang, H.-Y.; Fraser, M.; Li, W.; McAnulla, C.; McWilliam, H.; Maslen, J.; Mitchell, A.; Nuka, G.; Pesseat, S.; Quinn, A. F.; Sangrador-Vegas, A.; Scheremetjew, M.; Yong, S.-Y.; Lopez, R.; Hunter, S. InterProScan 5: Genome-Scale Protein Function Classification. *Bioinformatics* **2014**, *30* (9), 1236–1240. https://doi.org/10.1093/bioinformatics/btu031.

(96) Edgar, R. C. MUSCLE: Multiple Sequence Alignment with High Accuracy and High Throughput. *Nucleic Acids Research* **2004**, *32* (5), 1792–1797. https://doi.org/10.1093/nar/gkh340.
(97) Posada, D.; Crandall, K. A. Felsenstein Phylogenetic Likelihood. *J Mol Evol* **2021**, *89* (3), 134–145. https://doi.org/10.1007/s00239-020-09982-w.
(98) Le, S. Q.; Gascuel, O. An Improved General Amino Acid Replacement Matrix. *Molecular Biology and Evolution* **2008**, *25* (7), 1307–1320. https://doi.org/10.1093/molbev/msn067.
(99) Pang, A.-P.; Luo, Y.; He, C.; Lu, Z.; Lu, X. A Polyp-on-Chip for Coral Long-Term Culture. *Sci Rep* **2020**, *10* (1), 6964. https://doi.org/10.1038/s41598-020-63829-4.

879 **Figures**

880

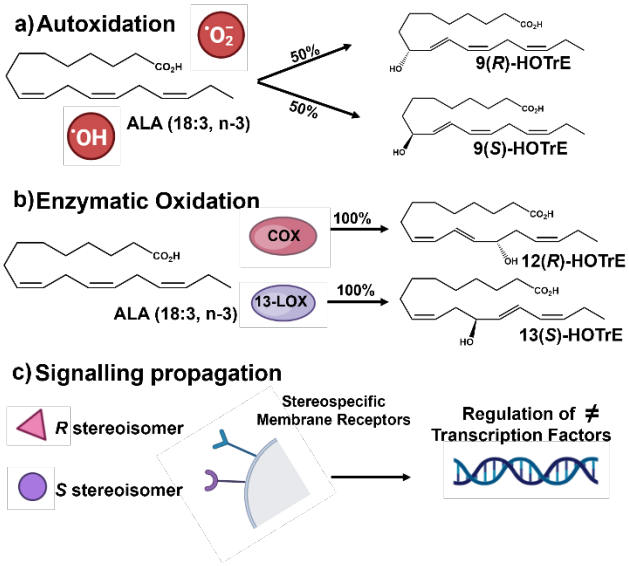

881

882 **Figure 1. Octadecanoid oxylipins can be formed *via* multiple synthetic routes**. **(a)**
883 Autoxidation in which free radicals (*e.g.,* hydroxyl radical (•OH and superoxide (•O_2^-)) or
884 singlet oxygen oxidize the fatty acid substrate. Notably, this process results in a racemic
885 mixture of the resulting mono-hydroxyl species. Here we only represent the products for the 9-
886 regioisomer, but the same process occures for the 9-, 10-, 12- and 15- regioisomers **(b)**
887 Enzymatic formation can result in stereo-selective formation of mono-hydroxy species (*i.e., R*
888 *vs S* enantiomer). **(c)** Propagation of signaling cascades can rely on binding with stereoisomer-
889 specific receptors. ALA = alpha linolenic acid; HOTrE = hydroxy-octadecatrienoic acid; COX
890 =cyclooxygenase; 13-LOX =13-lipoxygenase.

891

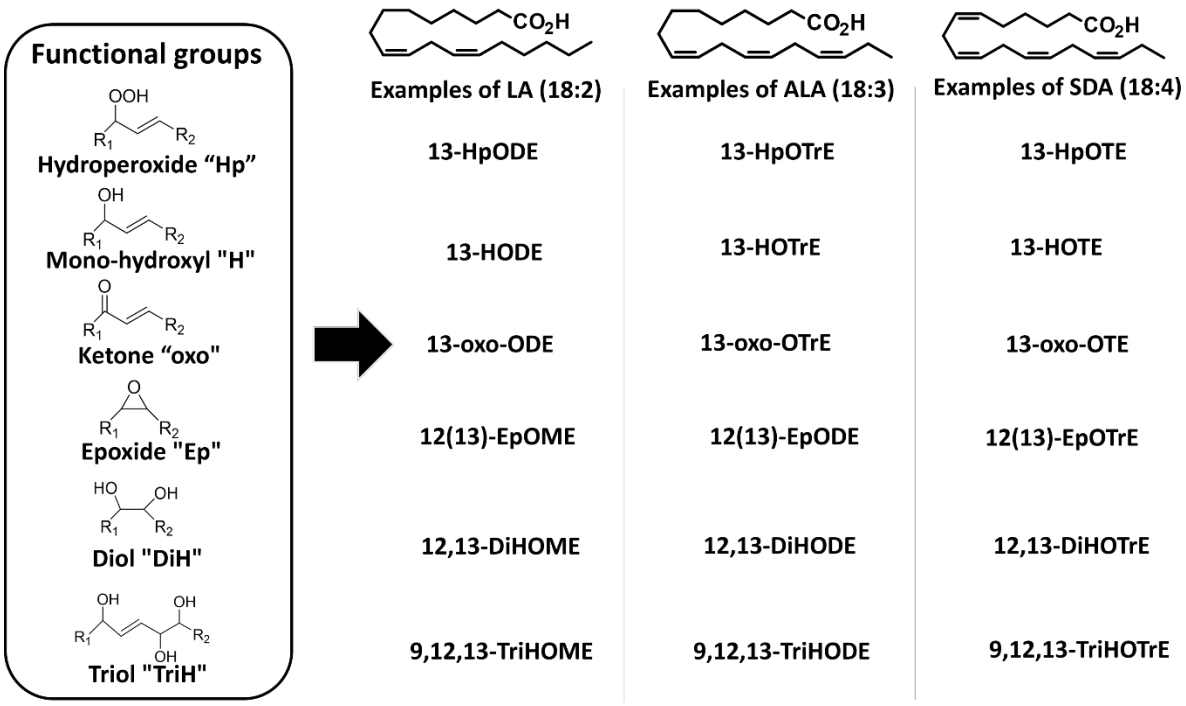

Figure 2. Abbreviated nomenclature system for octadecanoids. Compound names start with the positioning of the oxygenated moiety on the carbon backbone. The number(s) is followed by the abbreviation of the moiety (‘Hp' for hydroperoxides, ‘H’ for mono-hydroxyl, ‘DiH' for diols, ‘TriH' for triols, ‘oxo' for ketones, and ‘Ep' for epoxide) and by the alkyl chain length (for octadecanoids, a capital ‘O') and number of unsaturations (‘M': mono-unsaturated; ‘D': di-unsaturated; ‘Tr': tri-unsaturated; ‘T': tetra-unsaturated). The last letter indicates whether the compound is unsaturated (‘E' for enoic, unsaturated; ‘DA' for decanoic, saturated).

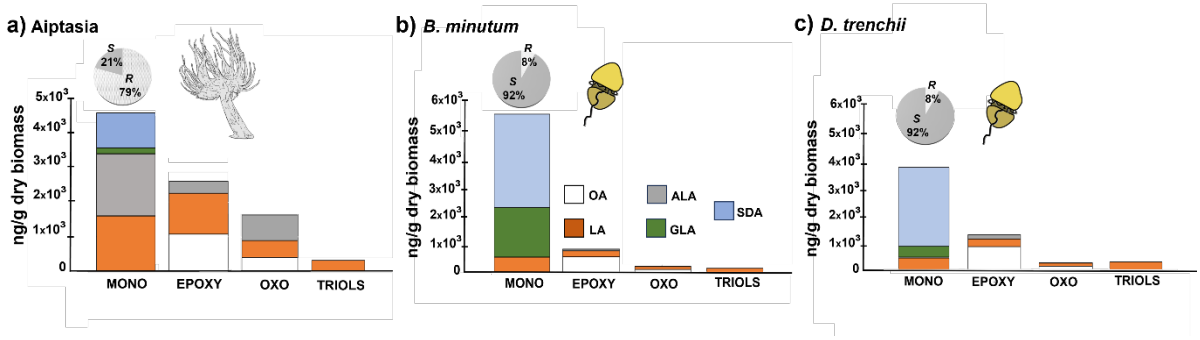

Figure 3. Quantitative overview of all quantified octadecanoids in the: a) aposymbiotic Aiptasia host; and cultured b) *Breviolum minutum* and c) *Durusdinium trenchii* symbionts. Octadecanoids are grouped as: mono-hydroxy octadecanoids (MONO=42 compounds), epoxides (EPOXY=26 compounds), ketones (OXO=9 compounds), and triols (TRIOLS=5 compounds). Percentages of the abundance of the *R* and *S* enantiomers were calculated for mono-hydroxy octadecanoids to highlight the distinct stereochemistry specificity between aposymbiotic anemones and dinoflagellate symbionts. Octadecanoid levels are presented as ng of octadecanoid per weight of dry biomass. The abundance of diols (n=2) was below 100 ng/g for all cases and so data for these are not presented in the graphs. Abbreviations: OA: oleic acid (18;1, n-9), LA (linoleic acid, 18:2, n-6), ALA (alpha-linoleic acid, 18:3, n-3), GLA (gamma-linoleic acid, 18:3, n-6), SDA (stearidonic acid, 18:4, n-3).

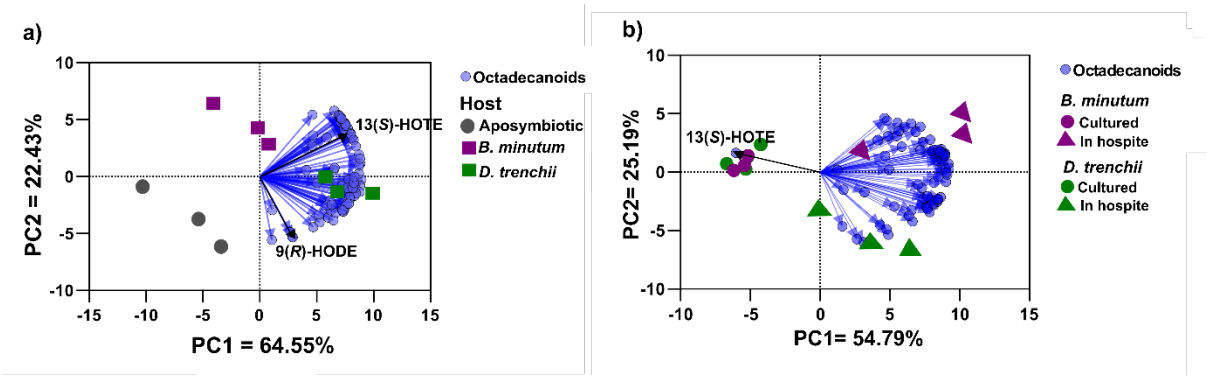

Figure 4. Principal component analysis of changes to the octadecanoid profile of (a) host and (b) symbiont caused by symbiotic state. The sea anemone Aiptasia was either aposymbiotic or colonized by the native symbiont *Breviolum minutum* or non-native symbiont *Durusdinium trenchii.* Blue circles represent individual octadecanoids and vector length is proportional to the individual contribution of each octadecanoid to the spatial distribution of sample replicates and groups. Compounds of interest are highlighted on the vectors and were further validated with a univariate test (see **Table S3** and **Fig. 5**). 13(*S*)-HOTE=13(*S*)-hydroxy-octadecatetraenoic acid. 9(*R*)-HODE=9(*R*)-hydroxy-octadecadienoic acid.

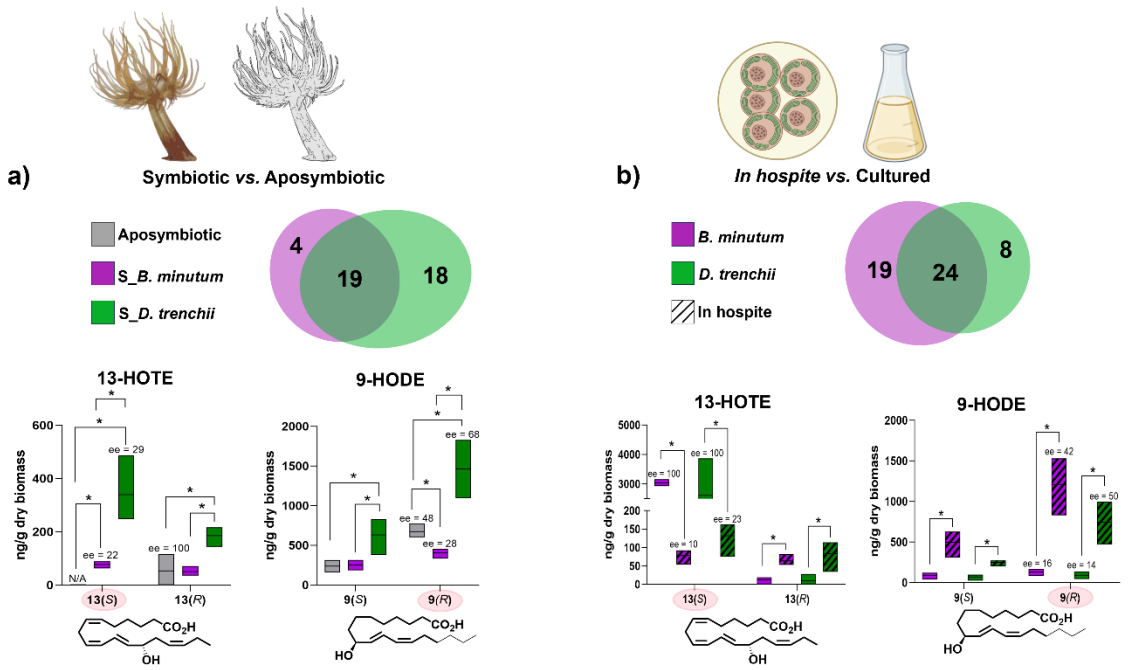

927

928 **Figure 5. Alterations to octadecanoid pathways in response to symbiosis: (a)** in the host
929 (Aiptasia) when symbiotic with the dinoflagellate symbionts *Breviolum minutum* and
930 *Durusdinium trenchii* (Symbiotic *vs*. Aposymbiotic); and **(b)** in the symbionts (*In hospite vs*.
931 Cultured). Venn diagrams indicate the number of octadecanoids significantly altered when in
932 symbiosis, including compounds shared by both species with pairwise fold-change differences
933 > 2; $p < 0.05$ with FDR (see **Tables S4** and **S5** for details). Species-specific changes are color-
934 coded. The enantiomeric excess values (ee %) for the *S* and *R* enantiomers of 13-HOTE and 9-
935 HODE are shown in each graph.

936

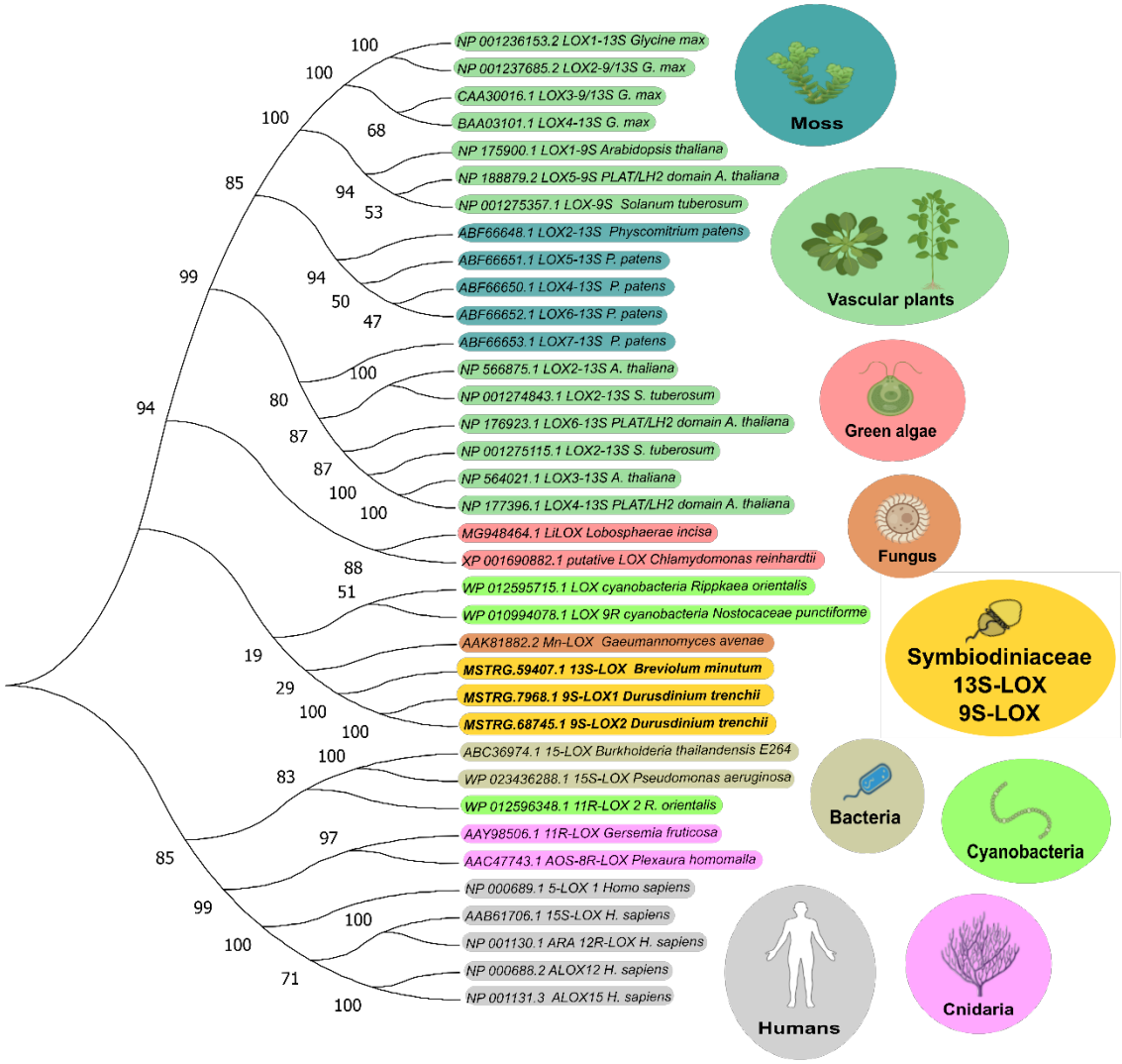

Figure 6. **Phylogenetic tree of lipoxygenases (LOXs) from different kingdoms and the novel LOXes in Symbiodiniaceae based on protein sequence homology.** Accession numbers were obtained from GenBank and are described in the Materials & Methods section.

Acknowledgements

We thank Prof. Miguel Mies (University of Sao Paulo, Brazil), Dr. Matthias Kellerman (Carl-von-Ossietzky University, Germany), Dr. Matthew Nitschke and Prof. Robert Keyzers for reviewing the manuscript. We also thank Prof. Blair Paul (Marine Biological Laboratory, Woods Hole, USA) for the assistance provided with the bioinformatics pipeline and Dr. Ellen Hornung (Georg-August-University, Germany) for the assistance with the LOX analysis. This manuscript is in memory of Professor Raymond Valentine (University of California, Davis, USA), may his incessant curiosity in understanding life always remains with us.

Funding

This research was supported by the Marsden Fund of the Royal Society Te Apārangi, grant number 19VUW086, awarded to S.K.D., C.A.O., A.R.G., D.J.S. and V.M.W., including a postgraduate scholarship awarded to M.T.B. I.F. acknowledges funding from the German Research Foundation (DFG) grant numbers GRK 1422 and GRK 2172. C.E.W. acknowledges support from the Swedish Research Council (2022-00796) and the Cayman Biochemical Research Institute (CABRI).

Contributions

M.T.B. and S.K.D. conceptualization; M.T.B. experimental design and sample processing, data analysis and manuscript writing; R.E.L. bioinformatics and data analysis; A.Q. and O.S. analytical sample runs; J.R.C. standards synthesis, M.H. standards synthesis and pathway analysis supervision; I.F. LOX analysis and pathway analysis supervision; I.F., C.A.O., A.R.G., D.J.S., V.M.W. manuscript editing; C.E.W. and S.K.D. funding, supervision and manuscript editing.

Corresponding authors

Craig Wheelock: craig.wheelock@ki.se
Simon Davy: simon.davy@vuw.ac.nz

Ethics declarations

Not applicable.

Consent for publication

Not applicable.

Competing interests

The authors declare that they have no competing interests.